SUPPORTING INFORMATION FOR

Hydrogen evolution reaction mediated by an all-sulfur trinuclear nickel complex.

Cyril Pieri,[a] Anirban Bhattacharjee,[b] Alexandre Barrozo,[a] Bruno Faure,[a] Michel Giorgi,[c] Jennifer Fize[d] Marius Réglier,[a] Martin Field,[d]* Maylis Orio,[a]* Vincent Artero[d] and Renaud Hardré [a]*

[a] Aix-Marseille Univ, CNRS, Centrale Marseille, iSm2, Marseille, France
[b] Socivolta Inc., 3 Place Ville Marie, Montréal, QC H3B 2E3, Canada.
[c] Aix Marseille Univ, CNRS, Centrale Marseille, Spectropole FR1739, Marseille, France
[d] Univ. Grenoble Alpes, CNRS, CEA, IRIG, Laboratoire de Chimie et Biologie des Métaux, 17 rue des Martyrs, 38000 Grenoble, France

1. Materials and methods

All solvents, chemicals and reagents were purchased either from Sigma Aldrich or Acros Organics and used without further purification. All solvents were distilled prior to use. Synthesis of (4-methyl-[1,2]dithiolan-4-yl)methanethiol was performed according to a procedure described by Pickett *et al.*[1,2] ^{1}H and ^{13}C NMR spectra were recorded on a Brüker Advance-300 instrument. Chemical shifts for ^{1}H NMR spectra are reported in ppm and are referenced relative to TMS. The ESI-MS spectra were recorded on a Bruker Esquire 3000 Plus or Amazon speed ion trap spectrometer equipped with an electrospray ion source (ESI). The

samples were analyzed in positive ionization mode by direct perfusion in the ESI-MS interface (ESI capillary voltage = 2 kV, sampling cone voltage = 40 V).

Thin-layer chromatography (TLC) was carried out using Merck silica gel F-254 plates (0.25 mm thick). Flash chromatography was carried out using Merck silica gel 60, 200–400 mesh. UV/Vis spectra were recorded on a Varian Cary 50 spectrophotometer.

2. Synthesis

2-bromoethyl-trityl-sulfide was prepared from NaH (730 mg, 18.2 mmol) dispersed in mineral oil (60%) washed with pentane and suspended in THF (20 ml). To this suspension maintained at 0°C, triphenylmethanethiol (5.03 g, 18.2 mmol) solubilized in THF (30 ml) was carefully added and stirred at room temperature for 30 min. This suspension was then cooled and maintained at 0°C for the slow addition of 1,2-dibromomethane (7.5 ml, 85.5 mmol) solubilized in THF (30 ml). The mixture was stirred at room temperature for 1 day and the solvent evaporated under vacuum. The resulting solid was dissolved in diethyl ether (200 ml), washed with brine (200 ml) and dried over anhydrous $MgSO_4$. Evaporation of diethyl ether under vacuum afforded a crude compound which was recrystallized in pentane to give 2-bromoethyl-trityl-sulfide as white solid (5.54 g, 80 %).

^{1}H RMN (300 MHz, $CDCl_3$), δ (ppm): 7.5-7.2 (m, 15 H), 2.9 (m, 2H), 2.8 (m, 2 H). ^{13}C RMN (300 MHz, $CDCl_3$), δ (ppm): 144.8, 129.9, 128.4, 127.3, 67.9, 34.6, 30.4.

4-methyl-4-((2-(tritylthio)ethylthio)methyl)-1,2-dithiolane (**2**).

NaH (120 mg, 2.4 mmol) dispersed in mineral oil (60%) was washed with pentane and suspended in THF (20 ml). To this suspension maintained at 0°C, (4-methyl-[1,2]dithiolan-4-yl) methane-thiol (800 mg, 4.8 mmol) solubilized in THF (20 ml) was carefully added. After a 30 min. stirring at room temperature, 2-bromoethyl-trityl-sulfide (1.85 g, 4.8 mmol) solubilized in THF (20 ml) was slowly added and the mixture stirred overnight at room temperature. A NH_4Cl saturated aqueous solution (20 ml) was added and the mixture extracted with ethyl acetate (3 x 30 ml). Organic phase was washed with brine (20 ml) and dried over anhydrous $MgSO_4$. Evaporation of ethyl acetate under vacuum afforded a crude compound which was chromatographed on SiO_2 (70 g, eluent toluene:pentane, 1:4) to give pure 4-methyl-4-((2-(tritylthio)ethylthio)methyl)-1,2-dithiolane (**2**) that was obtained as white solid (5.54 g, 66 %).

^{1}H RMN (300 MHz, $CDCl_3$), δ (ppm): 7.47-7.15 (m, 15H), 3.03 (d, 2H, ^{2}J = 11.4 Hz), 2.84 (d, 2H, ^{2}J = 11.4 Hz), 2.52 (s, 2H), 2.4 (2 x m, 2 x 2H), 1.23 (s, 3H). ^{13}C RMN (300 MHz, $CDCl_3$), δ (ppm): 145.1, 130.06, 128.4, 127.2, 67.6, 52.3, 49.6, 42.7, 33.8, 32.8, 24.8. MS $[M+NH_4]^+$: m/z = 486, $[M+NH_4]^+$: m/z = 491, $[M+K]^+$: m/z = 507.

2-((2-mercaptoethylthio)methyl)-2-methylpropane-1,3-dithiol (**3**).

Trifluoro acetic acid (3 ml) and triethylsilane (0.2 ml, 1.25 mmol) were slowly added, successively, to a degassed solution of 4-méthyl-4-((2-(tritylthio)ethylthio)méthyl)-1,2-dithiolane **2** (190 mg, 0.4 mmol) in dichloromethane (3 ml). The mixture was maintained under stirring overnight and dichloromethane was evaporated under vacuum. The solid residue was chromatographed on SiO2 (4 g, eluent toluene:pentane, 1:4) to give 2-((2-mercaptothioethyle)methyle)-2-methylpropane-1,3-dithiol **3** as a colorless oil (75 mg, 81 %).

^{1}H RMN (300 MHz, $CDCl_3$), δ (ppm): 3.9-3.5 (m, 10 H), 1.29 (3 x t, 3 x 1 H, t, 2H, J = 7 Hz), 1.04 (s, 3 H). DEPT135 RMN (300 MHz, $CDCl_3$), δ (ppm): 40.4 (CH), 38.0 (CH), 32.8 (CH), 25.2 (CH), 22.6 (CH_3). MS $[M+H]^+$: m/z = 229, $[M+Na]^+$: m/z = 251.

Nickel complex (**4**). Trifluoro acetic acid (3 ml) and triethylsilane (0.3 ml, 1.88 mmol) were slowly added, successively, to a degassed solution of 4-methyl-4-((2-(tritylthio)ethylthio)methyl)-1,2-dithiolane **3** (220 mg, 0.47 mmol) in dichloromethane (3 ml). The mixture was maintained under stirring overnight and dichloromethane was evaporated under vacuum. To the obtained residue dissolved in acetonitrile (10 ml), K_2CO_3 (300 mg, 2.35 mmol) was added. The mixture was maintained under stirring for 30 min. and $Ni(CH_3CN)_6(BF_4)_2$ (200 mg, 0.47 mmol) was slowly added. After 2 hours of stirring, the mixture was filtered and precipitated with diethyl ether. The crude solid was chromatographed on SiO_2 (8 g, eluent dichloromethane:methanol, 100:0 to 90:10) to give the complex **4** (45%) as a red solid.

^{1}H RMN (300 MHz, $CDCl_3$) δ (ppm): 3.50 (2H, m), 2.90 (2H, m), 2.66 (2H, m), 2.56 (4H, m), 2.25 (2H, d, J=26Hz), 1.80 (2H, d, 14 Hz), 1.61 (4H, m), 1.40 (2H, d, 14Hz), 1.23 (s, 6H). UV (DMF, 295 nm, 425 nm, 550 nm). MS $[M]^+$: m/z = 626, $[M+Na]^+$: m/z = 649.

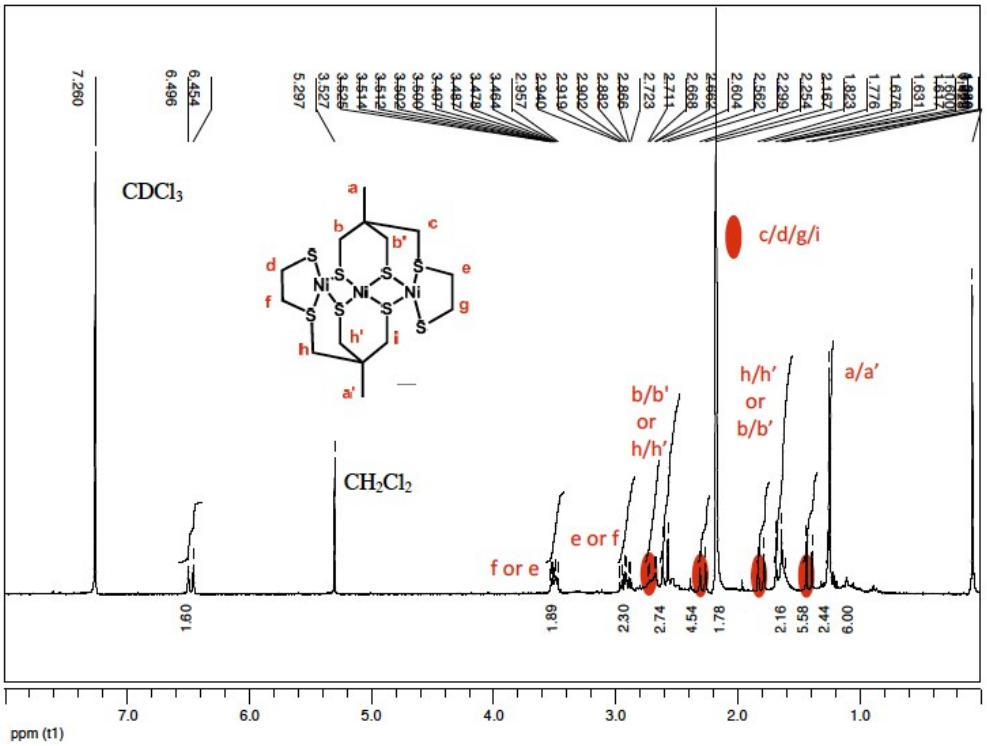

Figure S1. ^{1}H NMR spectrum of complex **4**. Conditions: 300 MHz, $CDCl_3$.

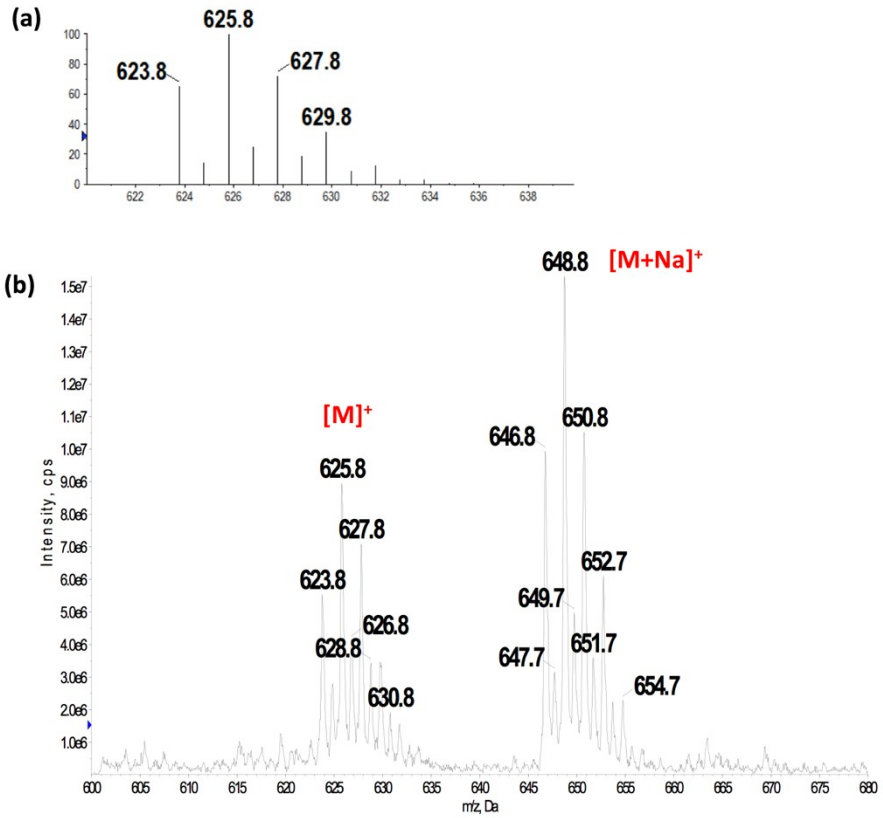

Figure S2. Simulated (a) and experimental (b) isotopic profile of complex **4**.

3. UV-vis spectroscopy

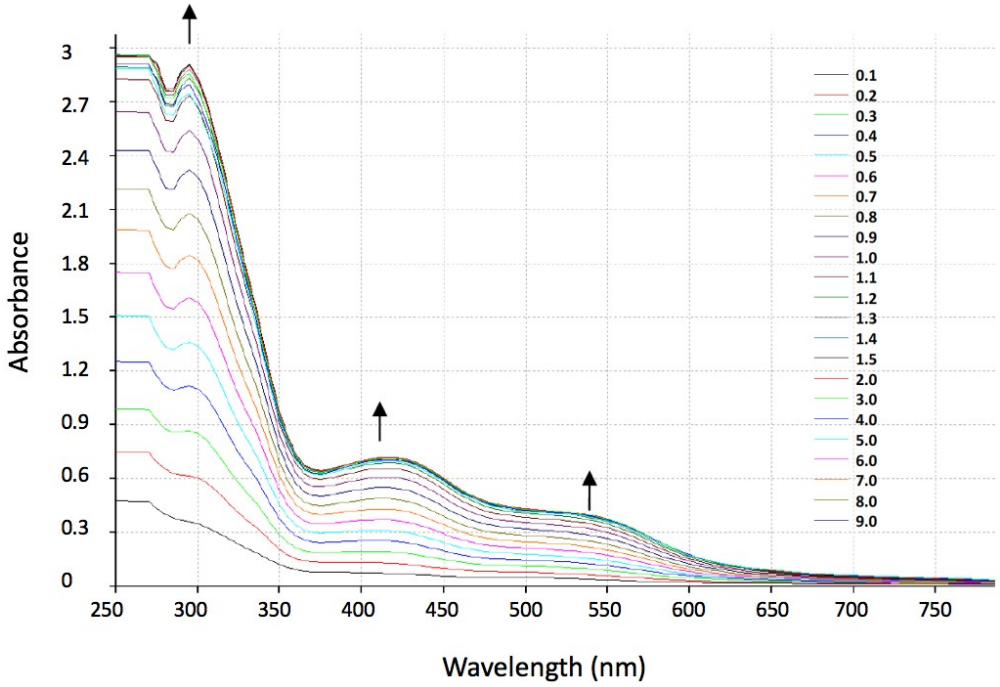

Figure S3. Molar extinction coefficients of a 1 mM solution of **3** at 540 (red) and 410 (blue) nm upon addition of increased amounts of $[Ni(H_2O)_6](ClO_4)_2$.

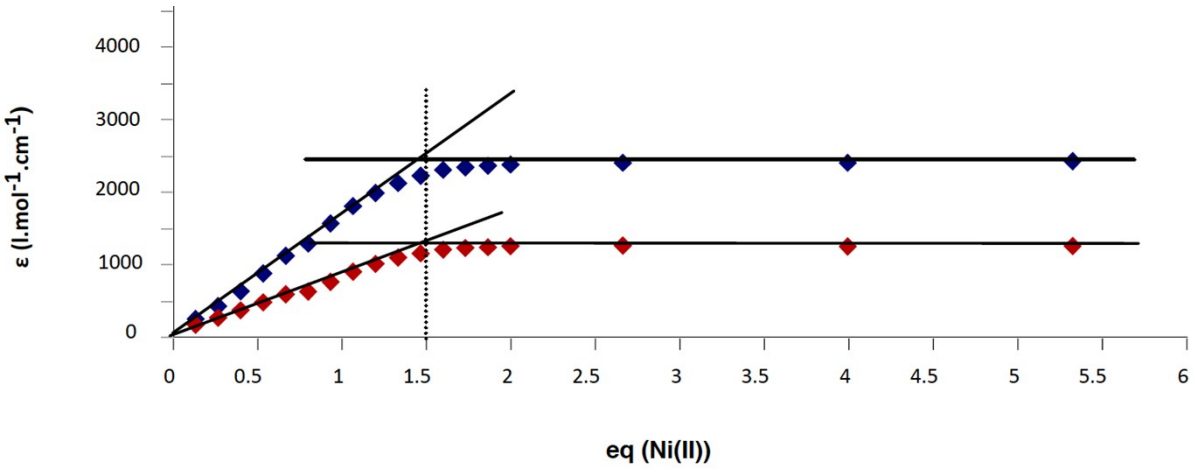

Figure S4. Evolution of the absorbance of a 1 mM solution of **3** upon addition of increased amounts of $[Ni(H_2O)_6](ClO_4)_2$.

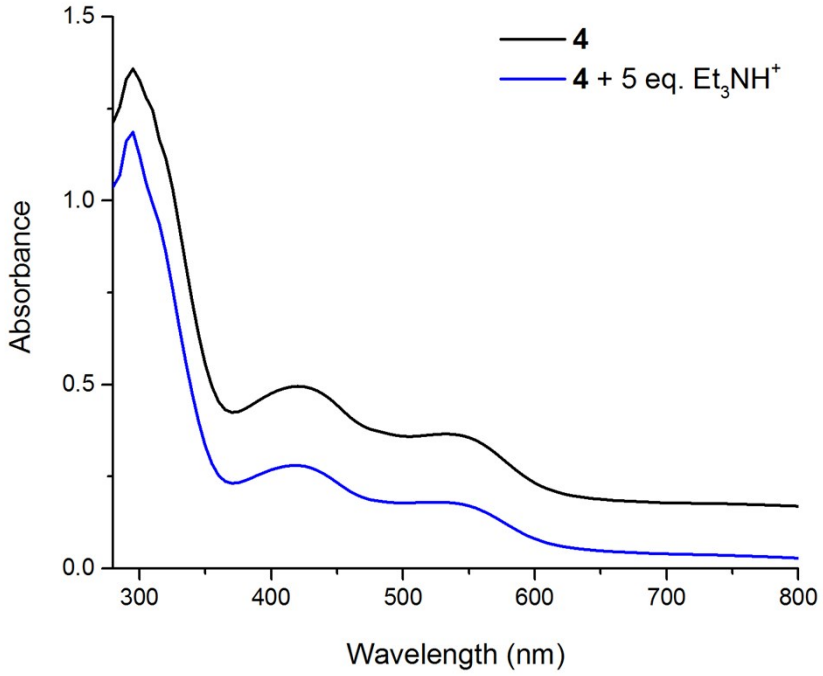

Figure S5. Electronic absorption spectra of 1 mM solutions of **4** in DMF in the absence (black line) and in the presence (blue line) of acid.

4. Single crystal X-ray Diffraction

Intensity data were collected on a Bruker–Nonius KappaCCD diffractometer using MoKα radiation (λ=0.71073 Å). Data collection was performed with COLLECT,[3] and cell refinement and data reduction with DENZO/SCALEPACK.[4] The structure was solved with SIR92,[5] and SHELXL-97[6] was used for full matrix least squares refinement. No absorption corrections were applied to the data. The hydrogen atoms were found experimentally and their Uiso parameters were fixed to 1.2Ueq (parent atom) for the carbons of the methylenes and to 1.5 Ueq (parent atom) for the methyls. Cristallographic data for compound **4** (CCDC 939713) can be obtained free of charge from The Cambridge Crystallographic Data Centre via: www.ccdc.cam.ac.uk/data_request/cif.

Table S1. Crystallographic data, details of data collection and structure refinement parameters for **4**.

Crystal colour and size/mm^3	Brown, 0.18*0.16*0.12
Formula	$C_{14}H_{26}S_8Ni_3$
Mw	626.96
Crystal system	orthorhombic
Space group	P b c n
a/Å	16.0517(3)
b/Å	12.6900(2)
c/Å	11.0788(2)
V/Å^3	2256.71(7)
Z	8
μ(Mo-Kα)/mm^{-1}	3.216
Unique refl., R_{int}	2877, 0.034
Refl. with *I>2σ(I)*	2431
R for *I>2 σ (I)*	0.026
Rw for *I>2 σ (I)*	0.048[a]
R (all data)	0.037
Rw (all data)	0.053[a]
Goodness of fit [all data]	1.049
Min/Max Residual Fourier/e. Å-3	-0.38/0.29

[a] $w = 1/[\sigma^2(Fo^2) + 1.872P]$ where $P = (Fo^2 + 2Fc^2)/3$

The structure of compound **4** is very compact and folded with a bowl shape and a small accessible cavity toward the central Ni-atom (mean width and depth equal to 3.4 Å and 4.9 Å, respectively). The Ni-S distances range from 2.1646(5) Å to 2.2001(6) Å, and the inter-metallic distances are equal to 2.7575(4) Å and 4.44736(8) Å for Ni1-Ni2 and Ni2-Ni2', respectively. The compactness and shape of the complex is also reflected in the geometry of the 5 and 6-membered rings. Indeed, ring puckering analysis[7,8] shows that cycle Ni2-S3-C6-C7-S4 is a half-chair ($\phi = 266°$) and the two 6-membered rings Ni1-S1-C3-C1-C4-S2 and Ni2-S2-C4-C1-C5-C3 can be described as a twisted boat and a boat respectively ($\theta = 82°$ and $\phi = 197°$, and $\theta = 106°$ and $\phi = 119°$ for the first and second cycles, respectively).

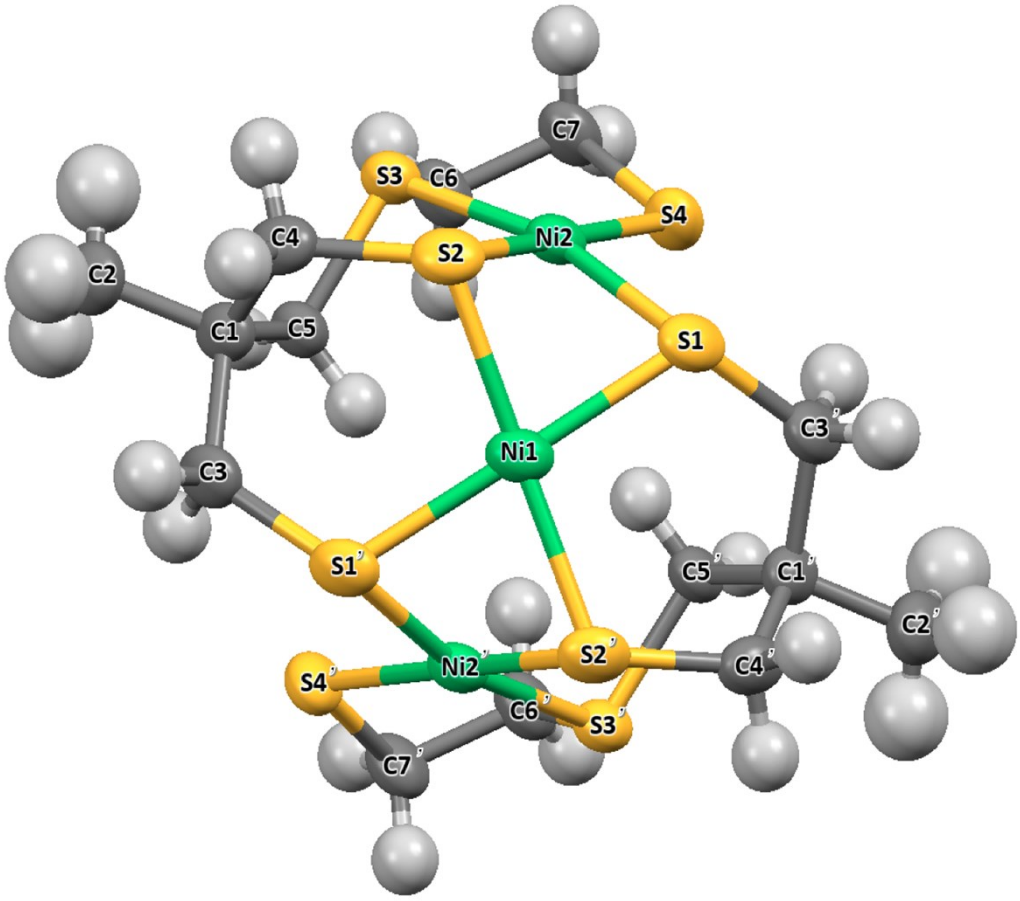

Figure S6. X-ray molecular structure of **4** with atom labeling scheme and ellipsoid parameters at 50% probability level.

Table S2. Selected bond distances and angles for compound **4**.

Distances in Å		**Angles in °**			
		Ni1-S1-Ni2	77.92(2)	Ni1-S2-Ni2	78.36(2)
Ni1 environnent					
Ni1-S1	2.1926(6)	S1-Ni1-S2	100.26(2)	S1-Ni1-S1’	167.96(3)
Ni1-S2	2.1649(5)	S2-Ni1-S1’	80.47(2)	S2-Ni1-S2’	173.12(4)
Ni2 environnent					
Ni2-S1	2.1930(6)	S2-Ni2-S1’	79.69(2)	S3-Ni2-S1’	165.51(2)
Ni2-S2	2.2000(6)	S3-Ni2-S2’	91.54(2)		
Ni2-S3	2.1725(6)	S4-Ni2-S1’	97.13(2)	S4-Ni2-S2	175.80(3)
Ni2-S4	2.1675(6)	S4-Ni2-S3’	92.13(2)		

N.B: label «’» stands for 2-x,y,1/2-z

5. Electrochemical Studies

Cyclic voltammetry experiments were performed using a BioLogic SP300 potentiostat and a three-electrode set-up consisting of a glassy carbon working electrode, a platinum wire counter electrode and a Ag/AgCl/3M $AgNO_3$ reference electrode. Ferrocene was used as an internal standard with $E^0(Fc^{+/0}) = 0.52$ V *vs.* Ag/AgCl for each measurement. All studies were performed in Ar-deaerated anhydrous DMF containing NEt_4ClO_4 as supporting electrolyte.

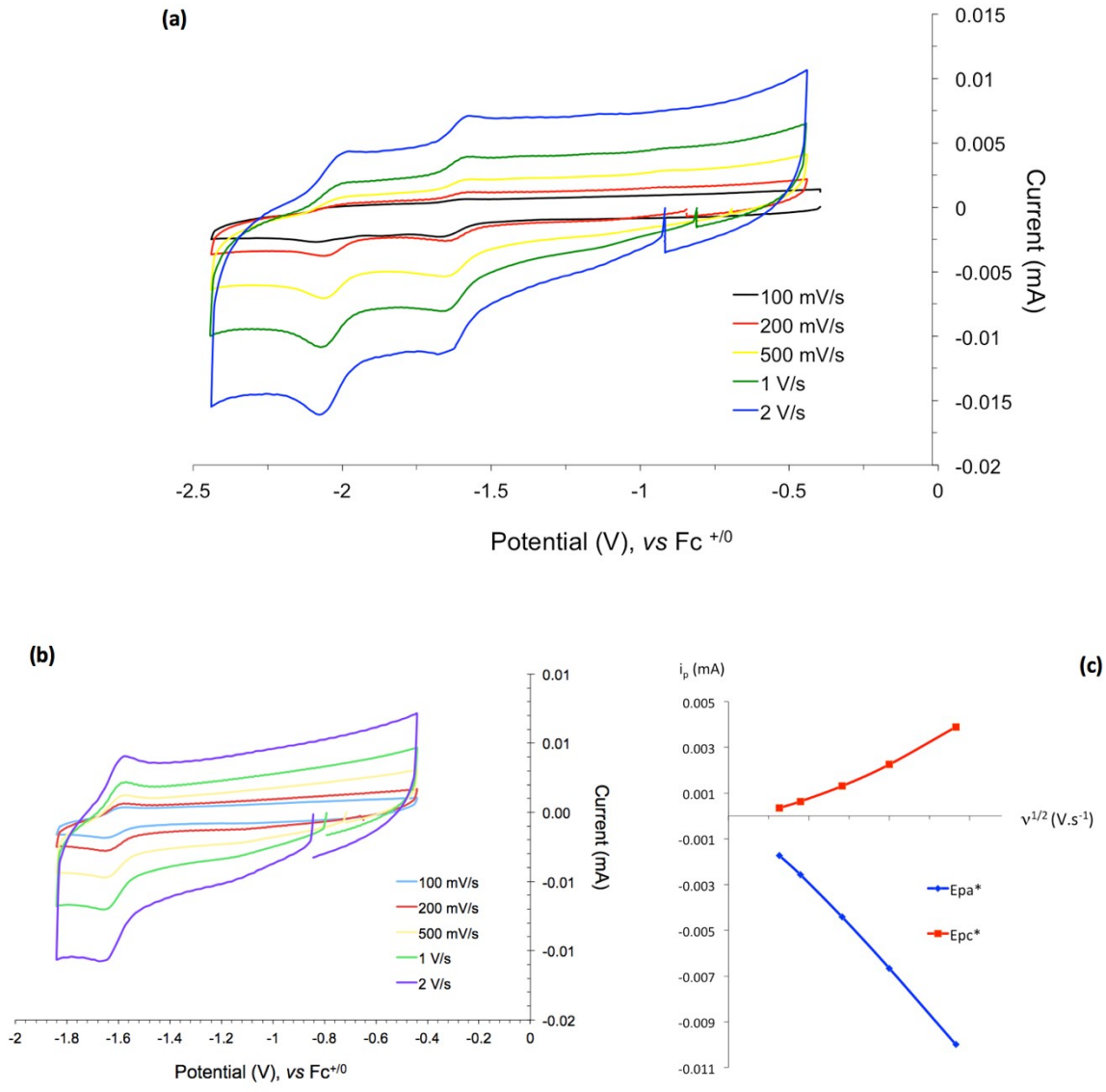

Figure S7. Cyclic voltammograms of **4** at a stationary glassy carbon electrode at different scan rates (v) in DMF with 0.1 M NEt_4ClO_4 as supporting electrolyte (a and b), and a linear plot of peak current vs. $v^{1/2}$ for anodic and cathodic waves of the first process (c).

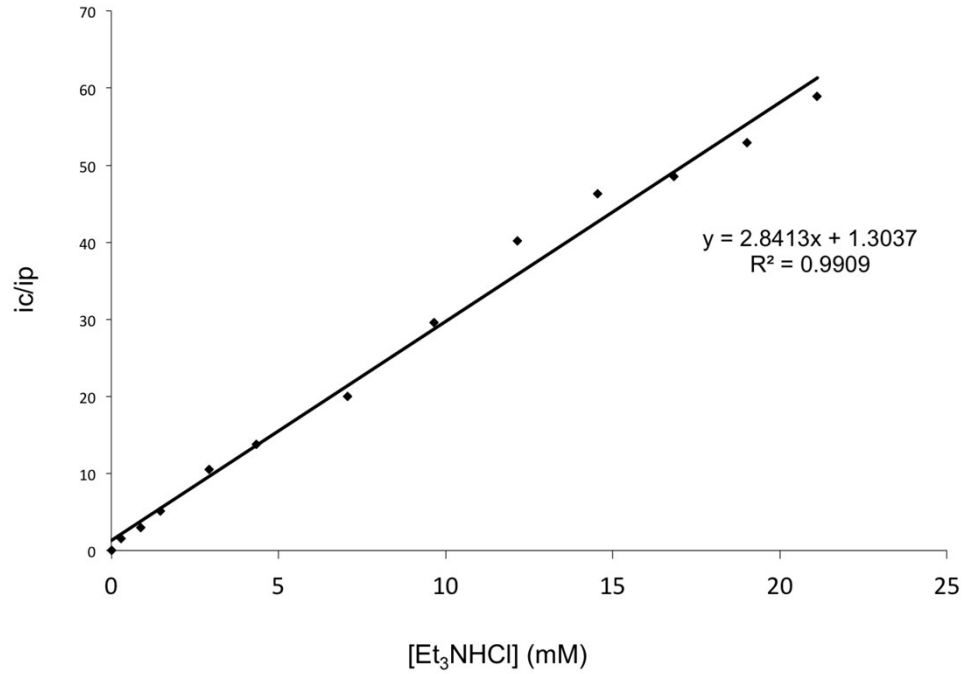

Figure S8. Plot of the ratio between the catalytic current and the peak current as a function of the proton source concentration.

Controlled potential electrolysis experiments were carried out in a two-compartment cell. The volume of solution (DMF, 0.1 M NBu_4BF_4) used in the working compartment of the cell was 10 ml. The working electrode used was a pool of mercury, separated from the coiled platinum wire counter electrode by a porous frit. Bulk electrolysis solutions were purged with N_2 gas for at least 20 min prior to electrolysis and stirred throughout the bulk electrolysis experiment. During the experiment, the cell was continuously purged with nitrogen (5 $mL.min^{-1}$) and the output gas was analyzed at two-minute intervals in a Perkin Elmer Clarus 500 gas chromatograph using a previously described setup.

6. DFT calculations

6.1 Electronic structures and spectroscopic properties of complex 4

All theoretical calculations used the ORCA program package.[9] Full geometry optimizations were performed using the GGA functional BP86[10-12] in combination with the def2-TZVP basis set[13] and by taking advantage of the resolution of the identity (RI) approximation in the Split-RI-J variant[14] with the appropriate Coulomb fitting sets.[15] Increased integration grids (Grid4 in ORCA convention) and tight SCF convergence criteria were used. To ensure that the resulting

structures converged to a local minimum on the potential energy surface, numerical frequency calculations were performed and resulted in only positive normal vibrations. Solvent effects were accounted for according to the experimental conditions. For that purpose, we used a DMF solvent (ε = 38.3) within the framework of the conductor-like polarizable continuum model (CPCM).[16] The relative energies were computed from the gas-phase optimized structures as a sum of electronic energy, relativistic and thermal corrections to the free energy. Electronic structures were obtained from single-point calculations using the hybrid functional B3LYP[17-18] together with the def2-TZVP basis set. Free energy differences for the redox potential calculations were extracted from the Gibbs free energies obtained from numerical frequencies calculations. Since experimental values are reported with respect to the ferrocene electrode in DMF, we need to shift our calculated absolute potentials. We calculated the Gibbs free energy difference for the ferrocene reduction in DMF, obtaining $\Delta G(Fcp^{+/0})$ = 5.02 eV. Optical properties were predicted from additional single-point calculations using the B3LYP functional and the range corrected hybrid functional CAM-B3LYP[19] together with the def2-TZVP basis set. Electronic transition energies and dipole moments for all models were calculated using time-dependent DFT (TD-DFT)[20-22] within the Tamm-Dancoff approximation.[23,24] To increase computational efficiency, the RI approximation[25] was used when calculating the Coulomb term and at least 40 excited states were calculated in each case. For each transition, difference density plots were generated using the ORCA plot utility program and were visualized with the Chemcraft[26] program. The same procedure was also employed to generate and visualize spin density plots as well as molecular orbitals.

Table S3. Calculated redox potentials for the first and second reductions of complex 4

	Redox potential (V)	
Functional	E_1	E_2
BP86	-1.84	-2.39
B3LYP	-2.02	-2.16
Exp.	-1.7	-2.1

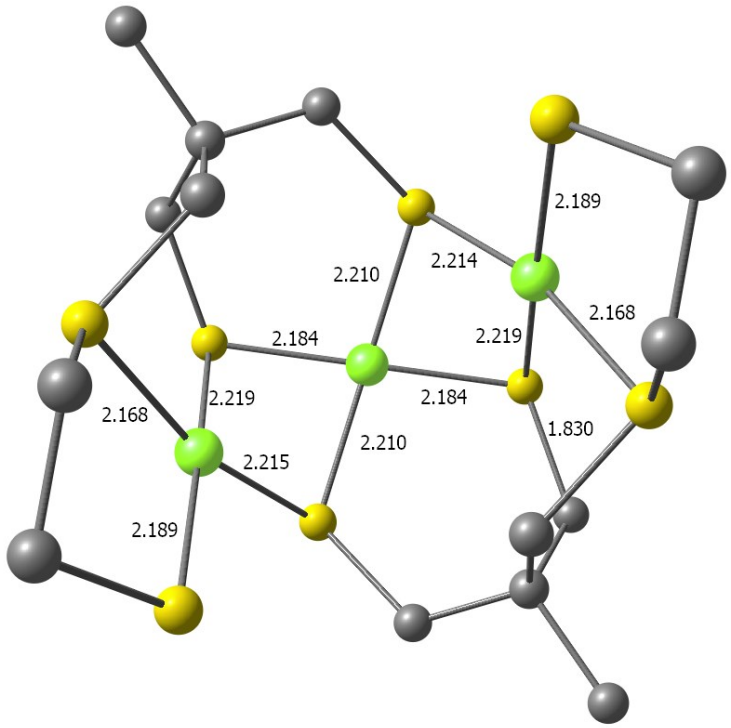

Figure S9. DFT-calculated geometry of **4**.

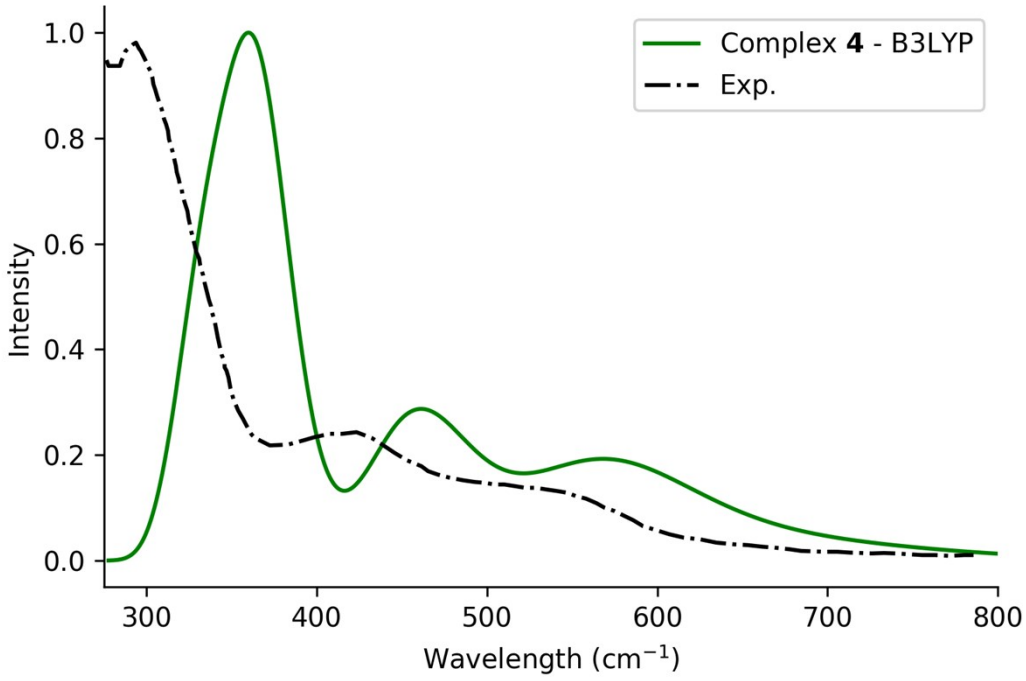

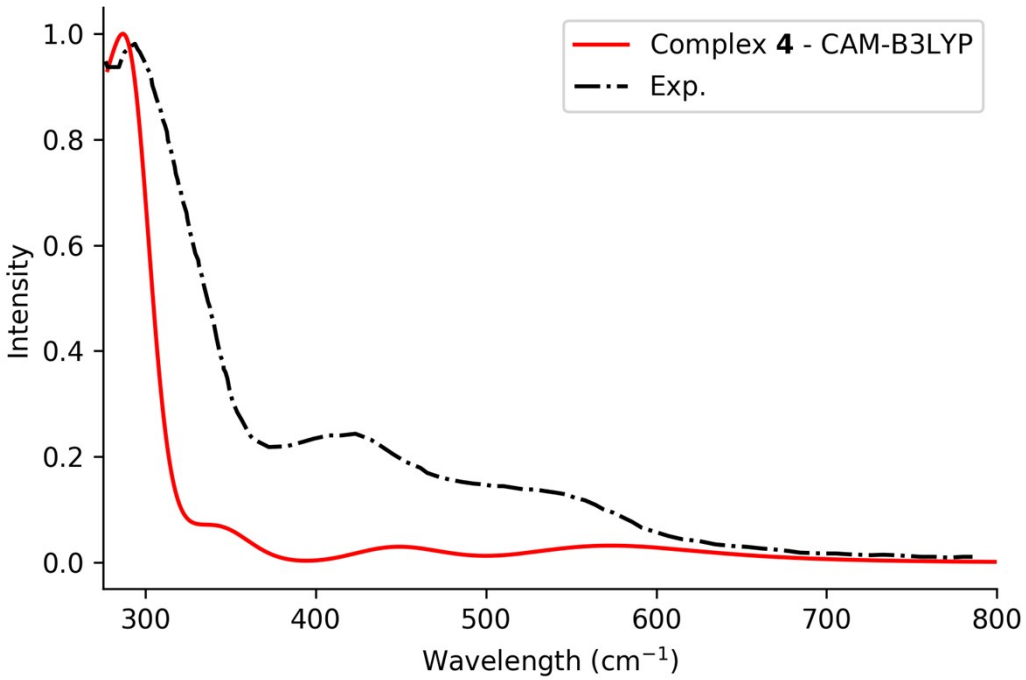

Figure S10. Comparison between experimental (dotted black line) and theoretical TD-DFT UV-Vis spectra for **4** using B3LYP (green line, top) and CAM-B3LYP (red line, bottom) functionals.

Table S4. Calculated electronic transitions of **4**.

	Transition	λ^{calc} (nm)	f^{calc} (nm)	Assignment
B3LYP	1	552	0.006	d-d
	2	457	0.013	MLCT
	3	334	0.036	MLCT
CAM-B3LYP	1	570	0.004	d-d
	2	448	0.006	MLCT
	3	286	0.031	MLCT

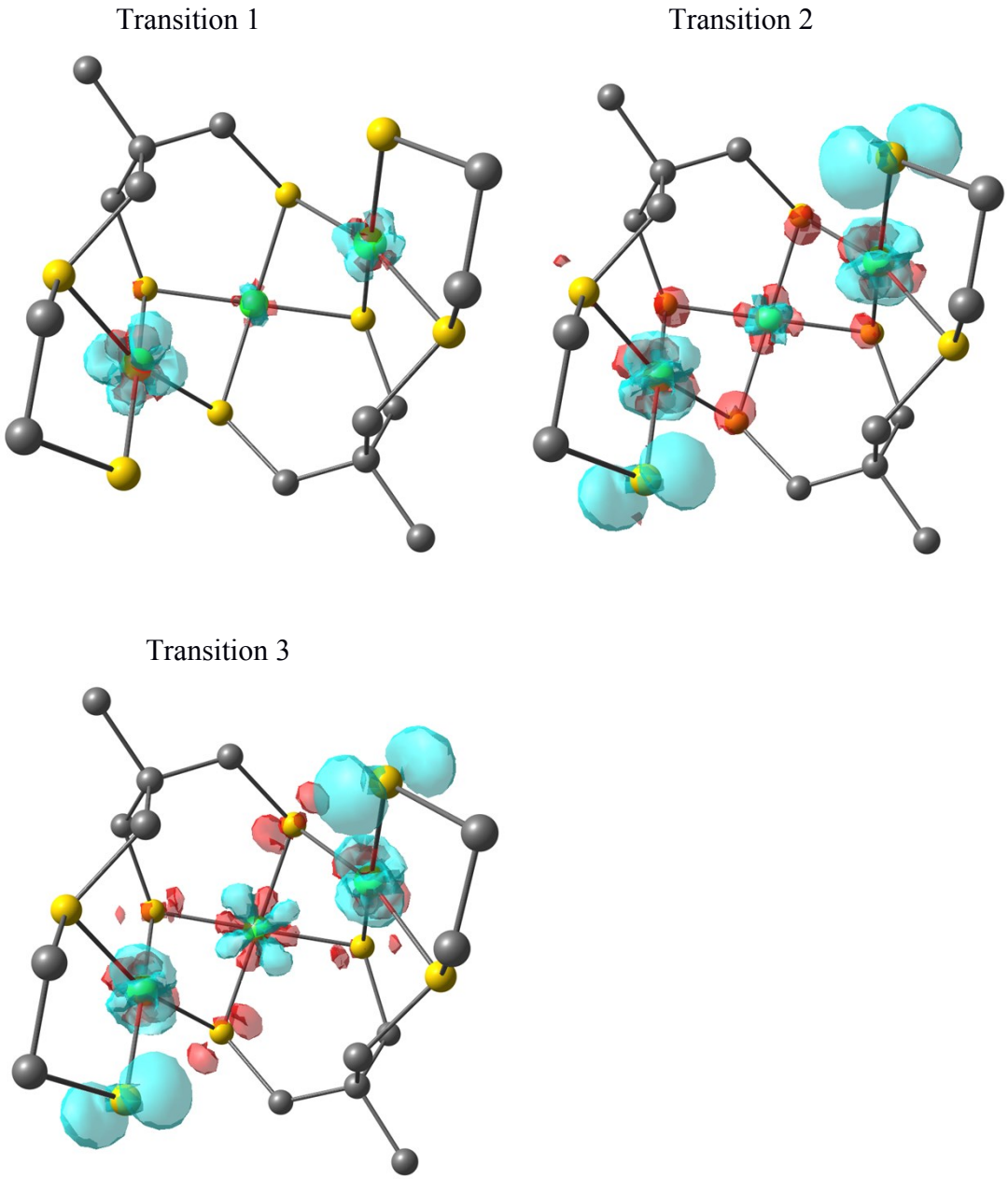

Figure S11. Difference electron density sketches for relevant transitions of **4**. Color scheme: positive in red and negative in blue

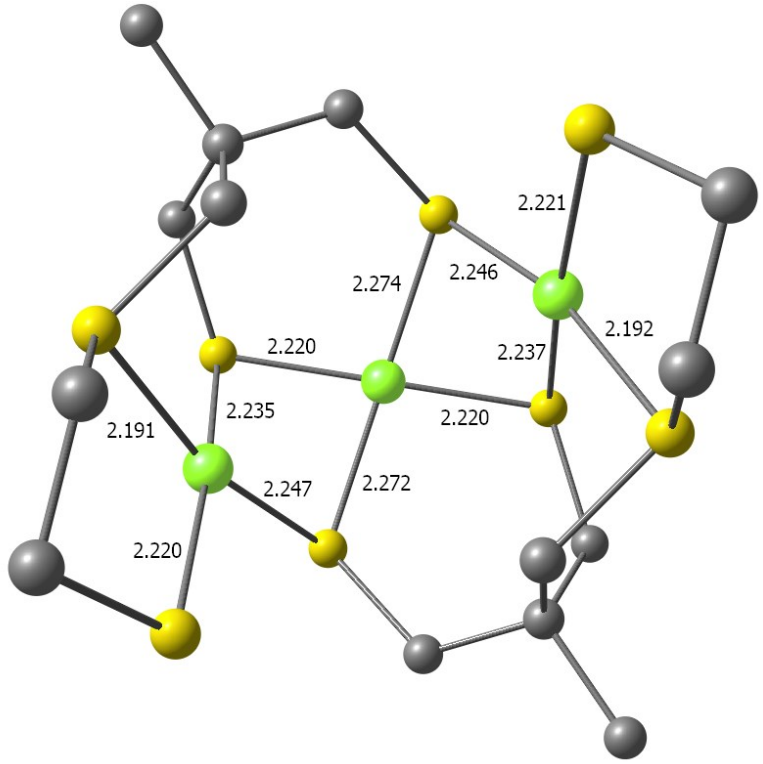

Figure S12. DFT-calculated geometry of the reduced species of **4** (doublet state, S=1/2).

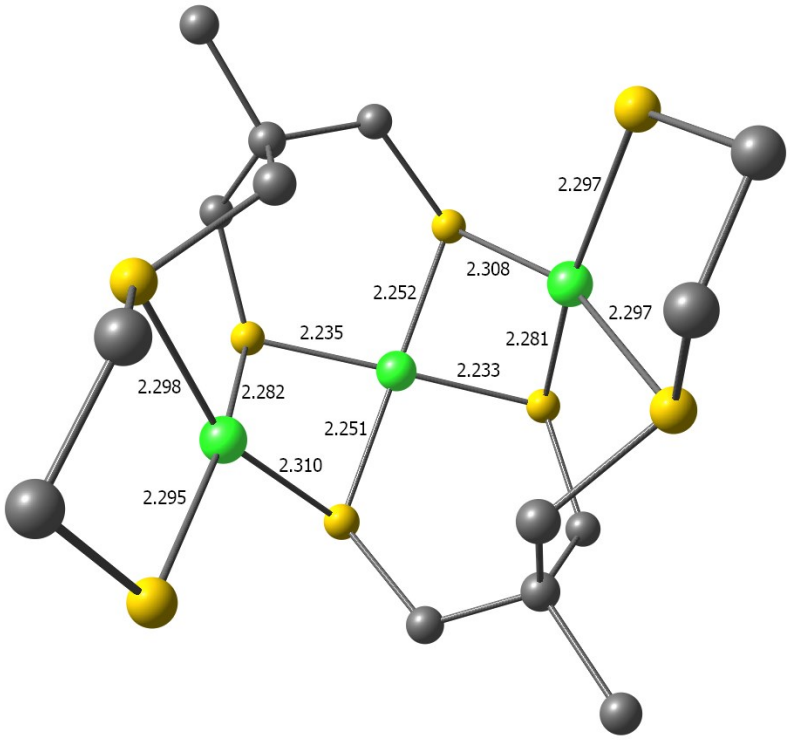

Figure S13. DFT-calculated geometry of the direduced species of **4** (triplet state, S=1).

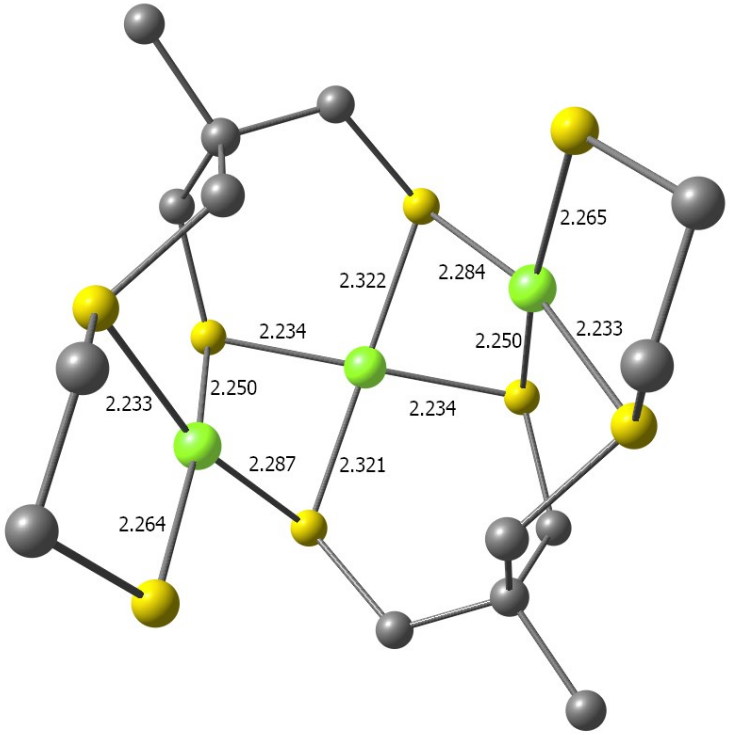

Figure S14. DFT-calculated geometry of the direduced species of **4** (singlet state, S=0).

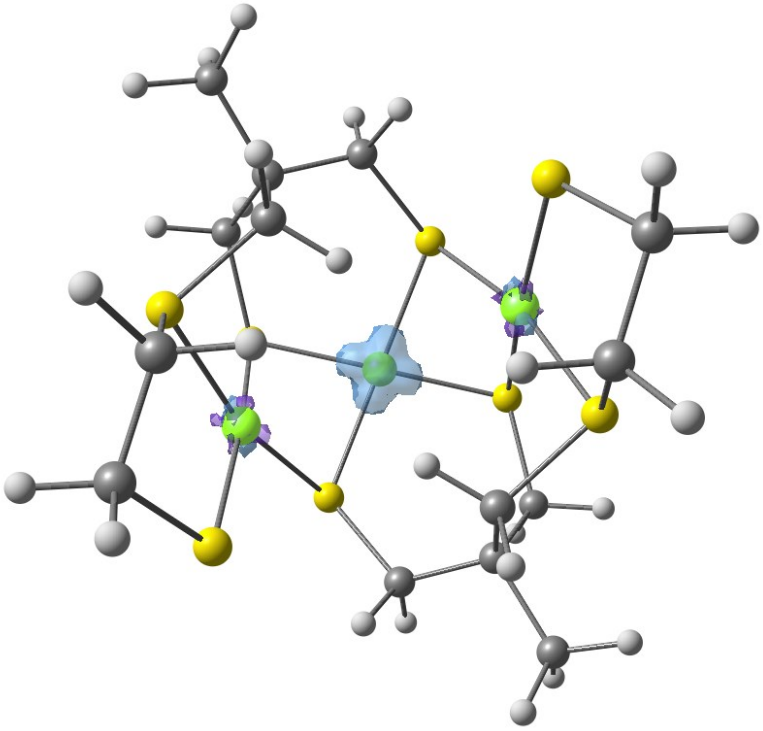

Figure S15. Spin density plot of the one-electron reduced species of **4** (doublet state, S=1/2).

The spin density changes substantially between the first and second reductions. In the first, the spin is localized on the central Ni. Upon a second reduction, the spin density migrates to the Ni centers on the sides, leaving the central Ni with no unpaired electrons. This rearrangement can be attributed to electrostatic repulsion between the two incoming electrons, which are stabilized in the Ni atoms away from the center. This process might not be reversible when oxidizing the reduced complex as removal of one electron might not cause reorganization of the electronic structure. This could explain the irreversibility observed in the cyclic voltammetry experiments.

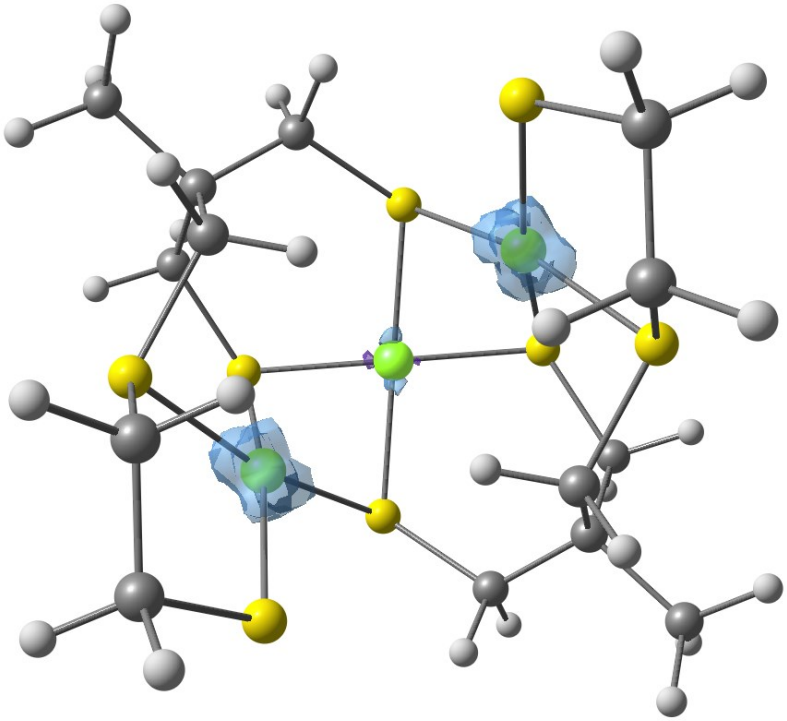

Figure S16. Spin density plot of the two-electron reduced species of **4** (triplet state, S=1).

Table S5. Cartesian coordinates of **4** (Q=0, S=0).

C	-2.53268	6.34014	9.88683
C	-3.84882	5.56056	10.12058
H	-4.49420	5.60356	9.23146
H	-4.40247	5.98200	10.97209
H	-3.63211	4.50449	10.33944
C	-2.92531	7.82687	9.71297
H	-3.31727	8.22191	10.66211
H	-3.72907	7.88623	8.96441
C	-1.92497	5.77834	8.58407
H	-2.54360	6.09056	7.73017
H	-1.93967	4.67827	8.61611

C	-1.62179	6.17308	11.12880
H	-2.22933	5.91847	12.00879
H	-1.06111	7.09119	11.34800
C	0.28415	4.72906	12.66963
H	0.18897	5.72788	13.11539
H	-0.33092	4.00736	13.22728
C	1.73709	4.31453	12.55514
H	1.82259	3.28341	12.18285
H	2.21862	4.36215	13.54290
C	4.55468	10.18794	10.98141
H	5.17675	10.51271	10.13485
H	5.12853	9.46140	11.57485
H	4.34875	11.06382	11.61437
C	3.22887	9.56148	10.48661
C	3.60909	8.27342	9.71793
H	4.02477	7.53226	10.41702
H	4.39248	8.52509	8.98789
C	2.59045	10.59792	9.53776
H	3.18542	10.66057	8.61497
H	2.61180	11.59137	10.01112
C	2.35167	9.20745	11.71336
H	2.98246	9.08766	12.60557
H	1.79191	8.27600	11.55709
C	0.49442	9.89263	13.75536
H	0.59995	8.79979	13.75743
H	1.12555	10.33308	14.54141
C	-0.95984	10.30598	13.85536
H	-1.05178	11.39890	13.93390
H	-1.41519	9.85940	14.75153
Ni	0.32844	8.25965	8.71893
Ni	1.16673	5.88007	9.86547
Ni	-0.46709	9.96860	10.74838
S	-1.68575	9.07026	9.13284
S	-0.20223	6.21862	8.15251
S	-0.38080	4.82051	10.95234
S	2.63743	5.47367	11.43452
S	2.34799	7.36150	8.71903
S	0.85462	10.35946	9.00954
S	1.11339	10.50819	12.13131
S	-1.89362	9.69206	12.38531

Table S6. Cartesian coordinates of **4** upon one-electron reduction (Q=(-1), S=1/2).

C	-2.53760	6.34822	9.88046
C	-3.82597	5.53375	10.14603
H	-4.48560	5.54184	9.26543
H	-4.38369	5.95267	10.99714
H	-3.57861	4.48702	10.37944
C	-2.96938	7.82613	9.71783
H	-3.35265	8.19970	10.67932
H	-3.79477	7.86283	8.98967
C	-1.93508	5.78330	8.56972
H	-2.55686	6.12022	7.72595
H	-1.98949	4.68440	8.59604

C	-1.60651	6.22724	11.10940
H	-2.20259	6.03219	12.01293
H	-1.02807	7.14873	11.26424
C	0.28889	4.79876	12.67650
H	0.23582	5.81655	13.08644
H	-0.34031	4.12176	13.27423
C	1.72935	4.33015	12.57249
H	1.77008	3.28385	12.23283
H	2.20487	4.38000	13.56346
C	4.53233	10.20236	11.01614
H	5.16788	10.55631	10.19059
H	5.11057	9.47811	11.60943
H	4.29591	11.06302	11.66012
C	3.23310	9.55646	10.47857
C	3.65236	8.27162	9.72317
H	4.05719	7.54449	10.44326
H	4.45906	8.53435	9.02095
C	2.59919	10.59840	9.52313
H	3.19799	10.63394	8.59990
H	2.66011	11.59364	9.98906
C	2.33654	9.16484	11.67656
H	2.95786	8.98386	12.56585
H	1.76065	8.25424	11.46055
C	0.49078	9.82879	13.73717
H	0.55564	8.73270	13.70576
H	1.13577	10.21764	14.53984
C	-0.95184	10.28465	13.86603
H	-1.00071	11.37889	13.97508
H	-1.40013	9.83693	14.76564
Ni	0.32880	8.25616	8.73645
Ni	1.18470	5.89702	9.84881
Ni	-0.48569	9.95481	10.72807
S	-1.75937	9.07904	9.09889
S	-0.19941	6.19016	8.11803
S	-0.38722	4.85618	10.96509
S	2.67965	5.41574	11.41744
S	2.41972	7.36768	8.68290
S	0.85031	10.39902	8.98991
S	1.11920	10.46824	12.12930
S	-1.93478	9.74290	12.39770

Table S7. Cartesian coordinates of **4** upon two-electron reduction (Q=(-2), S=0).

C	-2.53613	6.35014	9.87384
C	-3.79622	5.49918	10.15858
H	-4.46824	5.48644	9.28674
H	-4.35575	5.90480	11.01573
H	-3.51817	4.45975	10.39159
C	-3.00106	7.82110	9.73748
H	-3.33121	8.18111	10.72451
H	-3.86749	7.84550	9.05697
C	-1.94320	5.81932	8.53921
H	-2.56078	6.22023	7.71844
H	-2.04320	4.72322	8.51835

C	-1.58514	6.26170	11.08800
H	-2.17430	6.12920	12.00782
H	-0.98753	7.18095	11.18089
C	0.28507	4.83417	12.68675
H	0.25620	5.86410	13.06898
H	-0.34769	4.18695	13.31409
C	1.72036	4.33283	12.59981
H	1.73166	3.27696	12.28454
H	2.18115	4.38342	13.59825
C	4.50301	10.22759	11.04288
H	5.15213	10.59577	10.23357
H	5.08222	9.51324	11.64817
H	4.23518	11.08227	11.68300
C	3.23199	9.55646	10.47067
C	3.68630	8.26921	9.73918
H	4.04128	7.54402	10.48808
H	4.53379	8.52692	9.08358
C	2.60653	10.57875	9.48157
H	3.20207	10.55094	8.55402
H	2.70906	11.58947	9.90554
C	2.31365	9.13888	11.64061
H	2.92687	8.89118	12.51986
H	1.71523	8.25683	11.36747
C	0.49265	9.78807	13.72842
H	0.52389	8.69163	13.66163
H	1.14582	10.12927	14.54685
C	-0.94061	10.27672	13.88885
H	-0.95204	11.36991	14.02732
H	-1.37623	9.82563	14.79361
Ni	0.33012	8.24913	8.76682
Ni	1.21016	5.91226	9.83261
Ni	-0.51194	9.95108	10.70592
S	-1.82275	9.07010	9.05545
S	-0.19064	6.18342	8.09349
S	-0.39524	4.86556	10.97822
S	2.71542	5.36354	11.43171
S	2.48360	7.39338	8.64359
S	0.84203	10.41420	8.96965
S	1.12873	10.45275	12.13582
S	-1.97263	9.80222	12.43025

Table S8. Cartesian coordinates of **4** upon two-electron reduction (Q=(-2), S=1).

C	-2.50037	6.37812	9.90514
C	-3.75411	5.55413	10.28368
H	-4.45371	5.48797	9.43660
H	-4.28226	6.01845	11.13036
H	-3.47011	4.53133	10.57552
C	-2.96475	7.83291	9.67113
H	-3.29736	8.26215	10.62865
H	-3.81843	7.81506	8.97569
C	-1.94667	5.76260	8.59695
H	-2.63491	6.02442	7.77861
H	-1.94782	4.66537	8.68713

C	-1.51107	6.36498	11.09188
H	-2.06970	6.35076	12.03891
H	-0.872080	7.26015	11.06478
C	0.43217	4.97689	12.69290
H	0.53941	6.03700	12.96042
H	-0.20060	4.46691	13.43594
C	1.79953	4.31406	12.56064
H	1.67494	3.24071	12.34492
H	2.32641	4.39619	13.52353
C	4.46652	10.13362	11.12966
H	5.13923	10.54059	10.35950
H	5.01958	9.37359	11.70231
H	4.19540	10.95057	11.81595
C	3.19847	9.52054	10.48884
C	3.64996	8.28693	9.67597
H	4.01051	7.51210	10.36978
H	4.48286	8.59012	9.02236
C	2.61113	10.60703	9.55535
H	3.27760	10.70455	8.68449
H	2.61738	11.57425	10.08126
C	2.24551	9.04751	11.60966
H	2.83264	8.69096	12.46838
H	1.60689	8.22748	11.24858
C	0.33672	9.64481	13.67212
H	0.22415	8.56890	13.48011
H	0.99177	9.80191	14.54323
C	-1.02603	10.30393	13.85968
H	-0.894281	11.36987	14.10568
H	-1.532448	9.83008	14.71441
Ni	0.330225	8.26115	8.70593
Ni	1.253564	5.82082	9.73473
Ni	-0.556623	10.07749	10.65074
S	-1.760612	9.05767	8.96569
S	-0.23648	6.20203	8.04830
S	-0.39202	4.90075	11.04882
S	2.83195	5.11486	11.24433

6.2 Catalytic cycle of hydrogen evolution for complex 4

All calculations were conducted with the hybrid B3LYP and non-hybrid BP86 DFT functionals as previously used to study mimics of the active sites of [NiFe] and [FeFe] hydrogenases.[27-29] Geometry optimizations were performed with an extended TZVP basis set with extra polarization and diffuse functions in implicit solvent, with parameters appropriate for DMF. The geometry optimizations with the BP86 and B3LYP functionals gave structures that were very similar and so, in the figures and tables that follow, only the geometries obtained with the BP86 functional are listed. Free energy differences for the redox potential calculations were extracted from the Gibbs free energies obtained from numerical frequencies

calculations. Since experimental values are reported with respect to the ferrocene electrode in DMF, we need to shift our calculated absolute potentials. We therefore calculated the Gibbs free energy difference for the ferrocene reduction in DMF for both functionals thereby offering the possibility of cancelling systematic errors.

As a first step, the structure of Ni'S4'$_2$ determined by X-ray diffraction was optimized in DMF using two different DFT approximations: B3LYP and BP86. These optimized structures were then used as the starting point for geometry optimization, in DMF, of the first one-electron reduced intermediate in the cycle. In our previous studies, we found thermodynamic constants to depend quite significantly (~ ± 0.35 V for redox potentials and ± 2-3 units for pKa values) upon the DFT functional used and the solvent model employed. Roy et al.[30,31] found even higher discrepancies for the calculation of redox potentials using both hybrid and non-hybrid functionals with deviations of about ± 0.5 V observed for the redox potentials of thiolate complexes near -1.5 V vs Fc/Fc^+. With this our calculations for the Ni'S4'$_2$ system appear consistent with the experimentally determined value for the [Ni'S4'$_2$]/ [Ni'S4'$_2$]$^-$ couple (-1.6 V vs Fc/Fc^+).

In a second step, the protonation of [Ni'$_3$S4'$_2$]$^-$ with Et_3NH^+ yielding [Hni'$_3$S4'$_2$] was investigated. A number of different protonation sites were tried but the most stable was one in which protonation occurred on a terminal thiolate ligand coordinated to one of the peripheral Ni ions. This is in accord with the atomic charge populations of the [Ni'$_3$S4'$_2$]$^-$ complex as the terminal thiolate sulfurs are the most nucleophilic. This protonation reaction was calculated to be approximately isergonic. The next most favorable protonation site was on one of the peripheral Ni ions. This complex was less stable than the sulfur-protonated form by 28 and 61 kJ.mol^{-1} with the BP86 and B3LYP functionals, respectively. Overall the geometries and atomic charges of these two complexes are similar to those of the unprotonated reduced form and there is relatively little distortion at the protonation sites. There is, however, a marked change in the spin distributions of the two complexes as the unpaired electron shifts from the central nickel to the peripheral nickel that bears the proton or that is adjacent to the sulfur that is protonated.

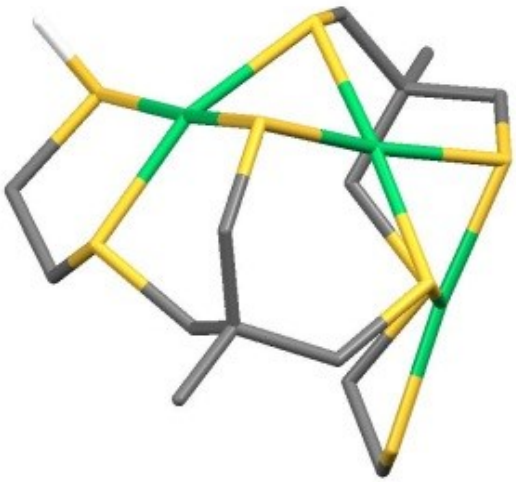

Figure S17. DFT-calculated structure for the sulfur-protonated reduced species [HNi_3'S4'$_2$].

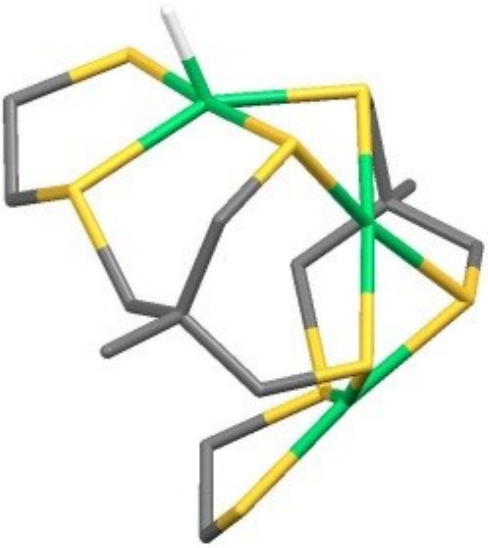

Figure S18. DFT-calculated structure for the metal-protonated reduced species [HNi_3'S4'$_2$].

Table S9. Cartesian coordinates of [HNi_3'S4'$_2$] (sulfur-protonated, Q=0, S=1/2).

C	1.72498	-2.84601	-0.0753
C	2.48918	-4.10819	0.40023
H	2.7268	-4.77551	-0.45295
H	1.88487	-4.68469	1.13017
H	3.44343	-3.82586	0.89114
C	0.35001	-3.31595	-0.61758
H	-0.24844	-3.73404	0.21775
H	0.52813	-4.13727	-1.34124
C	2.57207	-2.21551	-1.2083
H	2.50624	-2.85482	-2.11188
H	3.63957	-2.1856	-0.90735
C	1.50688	-1.8996	1.13521

H	1.47215	-2.4791	2.07946
H	0.56497	-1.32253	1.025
C	2.49058	0.04823	2.99504
H	1.39672	-0.02373	3.155
H	3.02097	-0.57175	3.74694
C	2.95091	1.49566	2.97752
H	4.0562	1.55627	2.8994
H	2.65178	1.99549	3.92167
C	-1.64953	2.84088	-0.1761
C	-2.39757	4.12955	0.25454
H	-2.59519	4.78846	-0.61542
H	-1.80237	4.70374	0.99359
H	-3.37165	3.87561	0.72116
C	-0.25221	3.27941	-0.68536
H	0.3304	3.72395	0.14751
H	-0.38538	4.06257	-1.45962
C	-2.48087	2.21645	-1.32912
H	-2.40202	2.87575	-2.21756
H	-3.55085	2.19536	-1.03549
C	-1.47386	1.91808	1.05761
H	-1.36994	2.52693	1.97733
H	-0.56803	1.28934	0.95072
C	-2.51112	0.03129	2.93437
H	-1.4102	0.03447	3.06381
H	-2.96061	0.65598	3.73172
C	-3.07941	-1.38226	2.99912
H	-4.18118	-1.38305	2.90234
H	-2.80667	-1.8621	3.95845
S	0.86725	2.03353	-1.4771
S	-2.10926	0.49853	-1.88743
S	-2.89898	0.76675	1.29009
S	-2.38826	-2.41739	1.61354
S	-0.76149	-2.11991	-1.50585
S	2.17377	-0.50724	-1.75741
S	2.85869	-0.6505	1.32194
S	2.15478	2.40471	1.5727
Ni	0.02422	-0.02528	-1.62001
Ni	2.08466	0.88393	-0.01686
Ni	-2.10146	-0.90258	-0.09179
H	-3.54415	-3.07207	1.30451

Table S10. Cartesian coordinates of [HNi_3'S4'$_2$] (metal-protonated, Q=0, S=1/2).

C	1.59014	-2.92244	0.01175
C	2.28776	-4.22201	0.48971
H	2.45384	-4.92002	-0.35554
H	1.6718	-4.74225	1.25117
H	3.27328	-3.99068	0.94372
C	0.16771	-3.313	-0.4641
H	-0.45247	-3.59356	0.41248
H	0.24845	-4.19987	-1.12434
C	2.42948	-2.37823	-1.16935

H	2.29595	-3.03749	-2.05053
H	3.50755	-2.39521	-0.90781
C	1.48198	-1.93877	1.20987
H	1.47889	-2.49789	2.16659
H	0.55834	-1.33067	1.1565
C	2.61965	0.02322	2.95976
H	1.5309	0.00222	3.1623
H	3.15313	-0.59432	3.71121
C	3.14015	1.44708	2.8733
H	4.2431	1.45826	2.75436
H	2.89503	1.99403	3.80669
C	-1.46701	2.90453	-0.19092
C	-2.13357	4.24044	0.22994
H	-2.32411	4.88747	-0.65008
H	-1.48415	4.79821	0.93457
H	-3.10352	4.05	0.7332
C	-0.07271	3.26063	-0.76614
H	0.56046	3.7075	0.02765
H	-0.1987	4.01896	-1.5654
C	-2.37213	2.29541	-1.29445
H	-2.29896	2.92193	-2.20638
H	-3.43238	2.32118	-0.97003
C	-1.29383	2.00186	1.05985
H	-1.07924	2.6238	1.95116
H	-0.44899	1.2973	0.9235
C	-2.42779	0.15492	2.97215
H	-1.32971	0.03288	3.05453
H	-2.78922	0.79407	3.80323
C	-3.13551	-1.19753	2.95115
H	-4.23633	-1.06603	2.90277
H	-2.90837	-1.75126	3.88536
S	0.96526	1.93905	-1.54172
S	-2.09171	0.56015	-1.8459
S	-2.79999	1.00195	1.38282
S	-2.56865	-2.26255	1.5543
S	-0.85213	-2.10505	-1.43389
S	2.11357	-0.66702	-1.75373
S	2.89524	-0.74744	1.30029
S	2.33376	2.33969	1.46447
Ni	0.00202	-0.06569	-1.59363
Ni	2.15214	0.77569	-0.06758
Ni	-2.31826	-0.81498	-0.08659
H	-3.73839	-1.17944	-0.22124

In a third step, the sulfur and nickel protonated reduced complexes were further reduced to yield $[HNi'_3S4'_2]^-$. This process was calculated to occur at potentials close to the one calculated for reduction of $[Ni'_3S4'_2]$. We note that the relative stabilities of the two isomers is inverted after this reduction step as the Ni-protonated form is now more stable than the sulfur-protonated form. The energy differences between the isomers are 76 and 24 $kJ.mol^{-1}$ with the BP86 and B3LYP functionals, respectively. The doubly-reduced sulfur-protonated complex displays

similar characteristics to its singly-reduced equivalent. The extra charge is accommodated mostly on the sulfurs and the major spin contributions are on the peripheral nickels in an antiparallel arrangement. By contrast, the doubly-reduced nickel-protonated complex shows considerable structural modification. Although the protonated nickel has maintained its square planar geometry, the hydrogen has replaced the terminal thioether sulfur as one of the ligands, the latter being ejected from the coordination sphere. The atomic charges indicate that the hydrogen has a charge of ~ –0.20, thereby confirming its hydride character.

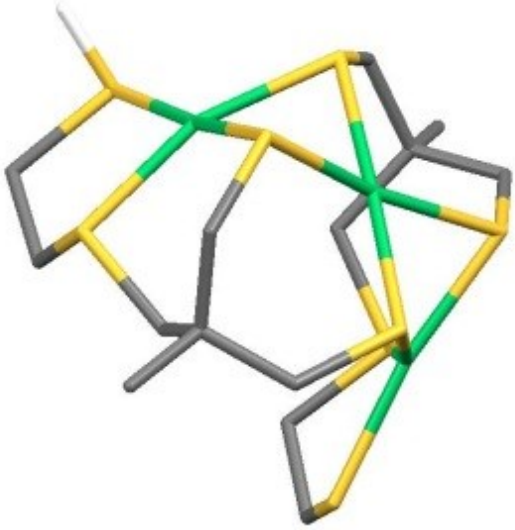

Figure S19. DFT-calculated structure for the sulfur-protonated direduced species $[HNi_3'S4'_2]^-$.

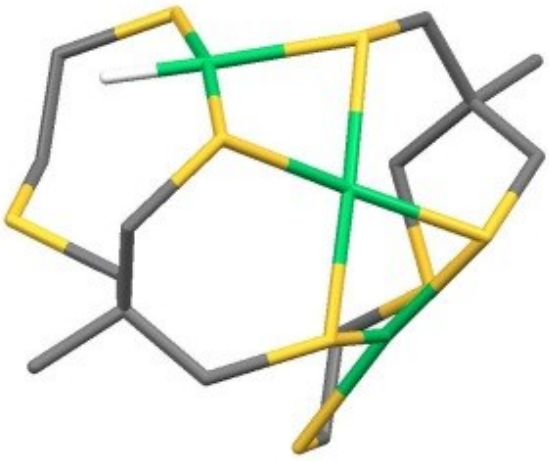

Figure S20. DFT-calculated structure for the metal-protonated direduced species $[HNi_3'S4'_2]$.

Table S11. Cartesian coordinates of $[HNi_3'S4'_2]^-$ (sulfur-protonated, Q=(-1), S=0).

C	-1.62067	-2.90445	0.12752
C	-2.35789	-4.17888	-0.35905
H	-2.60564	-4.84714	0.49145
H	-1.7311	-4.75188	-1.07349
H	-3.30496	-3.9112	-0.87218
C	-0.2513	-3.35336	0.69842
H	0.3539	-3.80306	-0.11617
H	-0.43226	-4.14755	1.45263
C	-2.50324	-2.28477	1.24556
H	-2.45054	-2.94658	2.1351
H	-3.5606	-2.27928	0.90794
C	-1.37594	-1.96556	-1.08229
H	-1.22349	-2.56417	-2.0036
H	-0.47937	-1.33461	-0.8998
C	-2.33742	-0.05629	-2.99499
H	-1.23109	-0.0091	-3.05196
H	-2.72211	-0.70896	-3.80693
C	-2.93921	1.34639	-3.04524
H	-4.04897	1.28099	-3.0548
H	-2.63366	1.83174	-3.99589
C	1.58725	2.88966	0.14414
C	2.31631	4.16811	-0.34459
H	2.54265	4.84791	0.50277
H	1.69224	4.72524	-1.0736
H	3.27472	3.90903	-0.84113
C	0.1979	3.32805	0.67613
H	-0.40464	3.71718	-0.17069
H	0.34891	4.15453	1.40201
C	2.45969	2.29527	1.28368
H	2.38277	2.96672	2.16415
H	3.52409	2.30193	0.96778
C	1.36878	1.93752	-1.0587
H	1.19467	2.52588	-1.98168
H	0.48483	1.28887	-0.88323
C	2.36222	0.04653	-2.95714
H	1.25612	0.00229	-3.01943
H	2.73638	0.67621	-3.78941
C	2.98325	-1.34439	-3.04103
H	4.08839	-1.29535	-3.02927
H	2.66098	-1.85378	-3.96957
S	-0.87743	2.09284	1.54624
S	2.12851	0.57617	1.87101
S	2.80973	0.81943	-1.34578
S	2.44718	-2.38315	-1.58558
S	0.83026	-2.09597	1.53284
S	-2.16898	-0.56101	1.82226
S	-2.77639	-0.80057	-1.36736
S	-2.36769	2.38948	-1.62343
Ni	-0.02171	0.00164	1.59891
Ni	-2.09604	0.85356	0.04648
Ni	2.12657	-0.85995	0.08131
H	3.66203	-2.97135	-1.37158

Table S12. Cartesian coordinates of $[HNi_3'S4'_2]^-$ (metal-protonated, Q=(-1), S=0).

C	2.17159	-2.49156	0.69947
C	3.08562	-3.45005	1.50546
H	3.48759	-4.25703	0.85932
H	2.52474	-3.92297	2.33753
H	3.94517	-2.89876	1.94034
C	0.92178	-3.29942	0.26308
H	0.30103	-3.52171	1.15609
H	1.26578	-4.26398	-0.16318
C	2.98996	-2.03608	-0.53481
H	3.07875	-2.88236	-1.24612
H	4.01918	-1.76178	-0.22361
C	1.72825	-1.32234	1.61963
H	1.72298	-1.64975	2.67868
H	0.7143	-0.95952	1.35887
C	2.26578	1.16332	2.9407
H	1.18479	0.958	3.06719
H	2.81832	0.84443	3.84874
C	2.51252	2.61561	2.5696
H	3.60058	2.83006	2.52268
H	2.07155	3.27968	3.34123
C	-2.05093	2.29728	-0.84618
C	-2.97321	3.54633	-0.78909
H	-3.12004	3.97669	-1.80105
H	-2.5351	4.33234	-0.14039
H	-3.97288	3.28718	-0.38534
C	-0.72711	2.81104	-1.47432
H	-0.27217	3.57503	-0.81145
H	-0.96898	3.30516	-2.4382
C	-2.74277	1.27438	-1.78497
H	-2.82641	1.72068	-2.79795
H	-3.76693	1.07095	-1.41457
C	-1.80074	1.74498	0.57673
H	-1.11581	2.42265	1.12482
H	-1.32714	0.74067	0.51071
C	-2.79758	0.47847	2.96733
H	-1.70516	0.61828	3.09938
H	-3.2929	0.93006	3.85297
C	-3.16526	-1.01326	2.9104
H	-4.21463	-1.12723	2.56739
H	-3.12093	-1.39716	3.95318
S	0.65184	1.65553	-1.90682
S	-1.99206	-0.4014	-2.01797
S	-3.34729	1.54687	1.56679
S	-2.05838	-2.12827	1.93905
S	-0.24885	-2.59897	-1.0005
S	2.38309	-0.60243	-1.51343
S	2.86252	0.13731	1.52168
S	1.70798	3.00938	0.94654
Ni	0.18858	-0.48081	-1.60013
Ni	1.95299	1.13803	-0.18703

Ni	-1.99997	-1.46936	-0.13287
H	-3.22291	-0.75433	0.23321

Finally, protonation of the reduced hydride species $[HNi'S4'_2]^-$ leads to formation of a dihydrogen complex $[(H_2)Ni'S4'_2]$. The H_2 molecule, with a H-H bond length of 0.84 Å, is side-on coordinated to Ni and also interacts with the sulfur atom of the decoordinated thioether group. The Ni, S and two H atoms are coplanar. The Ni-H distances are both 1.76 Å and the shortest S-H distance is 2.56 Å. The H-H bond is asymmetric with a partial charge of –0.097 on the hydrogen atom that is closest to the nickel centre. By contrast, the second hydrogen atom has a positive partial charge of +0.296. This structure corresponds to a true dihydrogen complex since the H-H bond length is shorter than 1.0 Å. The dihydrogen ligand is asymmetrically-bound to Ni and interacts with the thioether group as shown by the Mayer bond orders.

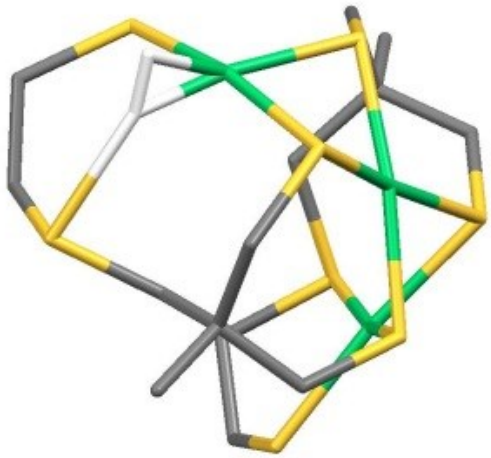

Figure S21. DFT-calculated structure for the diprotonated direduced species $[H_2Ni_3'S4'_2]$.

Table S13. Cartesian coordinates of $[H_2Ni_3'S4'_2]$ (metal-protonated, Q=0, S=0).

C	1.88629	-2.69665	0.50372
C	2.69188	-3.82722	1.19532
H	2.94622	-4.63384	0.4784
H	2.10943	-4.27445	2.02624
H	3.63834	-3.42816	1.61449
C	0.52354	-3.30627	0.08462
H	-0.09211	-3.50596	0.98665
H	0.70768	-4.27513	-0.42198
C	2.70495	-2.27174	-0.74052
H	2.66631	-3.07819	-1.50035
H	3.77012	-2.1378	-0.46069
C	1.65321	-1.54751	1.52407

H	1.6914	-1.94233	2.55884
H	0.67125	-1.05863	1.37667
C	2.5366	0.78194	2.93286
H	1.45378	0.66613	3.13451
H	3.1224	0.36392	3.77717
C	2.88919	2.22381	2.61372
H	3.98554	2.34637	2.49614
H	2.56227	2.88278	3.444
C	-1.81944	2.53402	-0.62983
C	-2.62294	3.84851	-0.42989
H	-2.77168	4.37132	-1.39617
H	-2.08674	4.535	0.25607
H	-3.62418	3.64633	0.00107
C	-0.47921	2.97044	-1.28137
H	0.06425	3.65124	-0.59495
H	-0.70945	3.53903	-2.20542
C	-2.64499	1.65645	-1.607
H	-2.72457	2.18	-2.5816
H	-3.67562	1.52308	-1.22182
C	-1.55341	1.85749	0.73531
H	-0.86561	2.48335	1.33805
H	-1.06427	0.87158	0.57917
C	-2.53401	0.45084	3.06349
H	-1.42888	0.50463	3.11946
H	-2.9356	0.90808	3.99068
C	-3.0266	-1.00265	2.97439
H	-4.11392	-1.03283	2.75585
H	-2.89184	-1.45732	3.97905
S	0.77849	1.72846	-1.82357
S	-2.06059	-0.04883	-2.02178
S	-3.09864	1.57524	1.70953
S	-2.11584	-2.13962	1.84551
S	-0.58397	-2.39966	-1.09235
S	2.24871	-0.72046	-1.61171
S	2.93368	-0.21423	1.42465
S	2.0143	2.77294	1.07558
Ni	0.08244	-0.35846	-1.62903
Ni	2.05431	0.96979	-0.17856
Ni	-2.24216	-1.25596	-0.16098
H	-3.33758	-0.21753	0.43358
H	-3.73617	-0.93247	0.07512

7. References

1. M. Razavet, S. C. Davies, D. L. Hughes, C. J. Pickett, *Chem Commun*, 2001, 847.
2. M. Razavet, S. C Davies, D. L. Hughes, J. E. Barclay, D. J. Evans, S. A Fairhurst, X. Liu, C. J. Pickett, *Dalton Trans*, 2003, 586.
3. B. V. Nonius, "Collect" Data Collection Software, 2001.
4. Z. Otwinowski, W. Minor, *Methods in Enzymology*, 1997, 276, 307.
5. A. Altomare, G. Cascarano, G. Giacovazzo, A. Guagliardi, M. C. Burla, G. Polidori, M. Camalli, *J. Appl. Cryst.*, 1994, 27, 435.
6. G. M. Sheldrick, *Acta Cryst.*, 2008, A64, 112.
7 D. Cremer & J.A. Pople, *J. Am. Chem. Soc.,* 1975, 97,1354.
8 J. C. A. Boeyens, *J. Cryst. Mol. Struct.,* 1978, 8,317.
9 F. Neese, *Wiley Interdiscip. Rev. Comput. Mol. Sci.*, 2012, 2, 73.
10. J. P. Perdew, *Phys. Rev. B*, 1986, 33, 8822.
11. J. P. Perdew, *Phys. Rev. B*, 1986, 34, 7406.
12 A. D. Becke, *Phys. Rev. A: At., Mol., Opt. Phys.*, 1988, 38, 3098
13. A. Schaefer, C. Huber and R. Ahlrichs, *J. Chem. Phys.*, 1994, 100, 5829.
14. F. Neese, *J. Comput. Chem.*, 2003, 24, 1740.
15. F. Weigend, *PhysChemChemPhys*, 2006, 8, 1057.
16. V. Barone, M. Cossi, *J. Phys. Chem. A*, 1998, 102, 1995.
17. A. D. Becke, *J. Chem. Phys.*, 1993, 98, 5648
18. C. Lee, W. Yang and R. G. Parr, *Phys. Rev. B*, 1988, 37, 785.
19. T. Yanai, D. P. Tew, N.H Handy, *Chem. Phys. Lett.* 2004, 393, 51.
20. M. E. Casida, In *Recent Advances in Density Functional Methods*, Chong, D.P. Ed. World Scientific: Singapore, 1995.
21. R. E. Stratmann, G. E. Scuseria, M. J.Frisch, *J. Chem. Phys.,* 1998, 109, 8218.
22. R. Bauernschmitt, R. Ahlrichs, *Chem. Phys. Lett.*, 1996, 454-464.
23. S. Hirata, M. Head-Gordon, *Chem. Phys. Lett.,* 1999, 314, 291.
24. S. Hirata, M. Head-Gordon, *Chem. Phys. Lett.,* 1999, 302, 375.
25. F. Neese, *J. Chem. Phys*., 2001, 115, 11080.
26. "Chemcraft - Graphical software for visualization of quantum chemistry computations.", *https://www.chemcraftprog.com*.
27. S. Canaguier, V. Fourmond, C. U. Perotto, J. Fize, J. Pecaut, M. Fontecave, M. J. Field, V. Artero, *Chem Commun*, 2013, 49, 5004.
28. S. Canaguier, M. J. Field, Y. Oudart, J. Pecaut, M. Fontecave, V. Artero*, Chem Commun,* 2010, 46, 5876.
29. V. Fourmond, S. Canaguier, B. Golly, M. J. Field, M. Fontecave, V. Artero, *Energy Environ Sci*, 2011, 4, 2417.
30. L. E. Roy, E. R. Batista, P. J. Hay, *Inorg. Chem.,* 2008, 47, 9228.
31. L. E. Roy, E. Jakubikova, M. G. Guthrie, E. R. Batista, *J. Phys. Chem. A,* 2009, 113, 6745.